Journal of Electroanalytical Chemistry 954 (2024) 118021

Contents lists available at ScienceDirect

Journal of Electroanalytical Chemistry

journal homepage: www.elsevier.com/locate/jelechem

New diamond coatings for peroxosulphate production

Laís G. Vernasqui [a,b], Géssica O. S. Santos [b,c], Alberto Rodríguez-Gómez [b], Marcos R. V. Lanza [c], Neidenei G. Ferreira [a], Manuel A. Rodrigo [b,*]

[a] Laboratório Associado de Sensores e Materiais, Instituto Nacional de Pesquisas Espaciais (INPE), Av. dos Astronautas, 1758, 12227 010 São José dos Campos, SP, Brazil

[b] Electrochemical & Environmental Engineering Lab, TEQUIMA Research Group, Faculty of Chemical Sciences and Technologies, University of Castilla La Mancha, Edificio Enrique Costa Novella, Campus Universitario s/n, 13071 Ciudad Real, Spain

[c] Sao Carlos Institute of Chemistry, University of São Paulo, São Carlos, São Paulo 13566-590, Brazil

ARTICLE INFO

Keywords:
Peroxosulphate
Caro's acid
Diamond electrodes
Electrolysis

ABSTRACT

In this work new diamonds coating, named as nanocrystalline diamond (ND) and ultrananocrystalline diamond (UND) are evaluated for the production of peroxospecies derived from the electrolysis of sulphuric acid and their performance is compared to that of a commercial diamond coating widely used in the literature and well-known by its outstanding performance. The oxidant production was tested at two different current densities and significant differences were found in oxidant production between the electrodes applied in the different conditions studied. Results demonstrate that when the lowest current is applied (25 mA cm^{-2}), the ND and UND electrodes are more efficient in the persulfate formation. For ND electrode, this behavior can be explained in terms of the promoted hydroxyl radical formation at these conditions. However, the UND electrode presented different behavior: the lesser hydroxyl formation and highest peroxospecies formation. This behavior may be attributed to the sum of two factors: the high sp^2 content in the diamond film and its porosity, that can increase the sulphate adsorption at the surface that, in turn, facilitates the persulfate generation. This behavior can be proved by the Tafel plots and are explained by the electrode's features discussed by Raman spectra. When the operation current is increased to harsher conditions (300 mA cm^{-2}), the commercial electrode increases importantly the production of the studied oxidant. One more time it can be attributed to the hydroxyl radical generation at this condition. Considering the energy consumption and the process efficiency, it can be concluded that the UND electrode is more attractive for this application in the studied conditions.

1. Introduction

Over the last decades, an increasing interest in the production of oxidants using electrochemical technology has been noticed. Applications of oxidants in disinfection, removal of pollutants, as bleaching agents or, alternatively, in many other industrial processes help to explain this interest. Electrolysis is, perhaps the technology that best suit to this production and, in addition to the well-known production of the chlorine commodity, there are many licensed processes in operation nowadays and much more under research & development at different technology readiness levels (TRL) [1].

Oxidants like ozone, hydrogen peroxide, chlorine dioxide and different peroxocompounds are in focus nowadays [2]. However, one of the oxidants that currently is attracting a great deal of attention is peroxosulphuric acid [3]. Under this name, three different types of products are included. The two first, peroxomonosulphuric acid (or alternatively peroxymonosulphuric acid or caro's acid) and peroxodisulphate anion are real peroxocompounds, with a structure shown in Fig. 1 characterized by including a real peroxo group —O—O— interacting with sulphur atoms [4].

In addition, as for many other peroxocompounds (a family of products in which peroxocarbonates, peroxophosphates and peroxonitrates area also included) different products consisting of mixtures sulphuric acid/hydrogen peroxide with different degrees of stabilization are also marketed, although they are not real peroxocompounds because they lack the group peroxo —O—O— in their structure. In fact, in the commercial product this group is associated only to the hydrogen peroxide, being much less active from the oxidation perspective.

Under acidic conditions, the primary species formed by electrolysis is the Caro's acid, which has an outstanding reduction potential of 2.5 V *vs*

* Corresponding author.
E-mail address: manuel.rodrigo@uclm.es (M. A. Rodrigo).

https://doi.org/10.1016/j.jelechem.2023.118021
Received 5 September 2023; Received in revised form 19 December 2023; Accepted 29 December 2023
Available online 30 December 2023

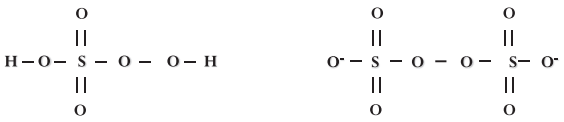

Fig. 1. Molecular structure of peroxymonosulphuric acid (Caro's acid) and diperoxosulphuric acid (persulphate).

SHE. First application of diamond coatings in the production of Caro's acid was proposed by the group of Comninellis more than two decades ago [5] and from that moment many other contributions have been made regarding the suitability of these electrodes for the production of this interesting oxidant [6]. Two mechanisms have been proposed for the electrochemical production of the Caro's acid. The first is shown in Eq. (1) and consists of the direct electrolysis of sulfuric acid on the surface of the diamond coating.

$$H_2SO_4 + H_2O \rightarrow H_2SO_5 + 2H^+ + 2e^- \quad (1)$$

The second is a mediated process that starts with the production of hydroxyl radicals on the surface of the diamond anode (Eq. (2)) and continues with the successive attack of sulphuric acid by these radicals (as shown in Eqs. (3) and (4)). The massive production of hydroxyl radicals that do not interact with the surface of the diamond coating explains the feasibility of this mechanism.

$$H_2O \rightarrow {}^{\bullet}OH + H^+ + e\text{-} \quad (2)$$

$$H_2SO_4 + {}^{\bullet}OH \rightarrow HSO_4^{-\bullet} + H_2O \quad (3)$$

$$HSO_4^{\bullet} + {}^{\bullet}OH \rightarrow H_2SO_5 \quad (4)$$

The reduction product of the Caro's acid is sulphate, which can be further regenerated to produce the oxidant. Decomposition is favored by the presence of activators that allow transforming the Caro's acid into sulphate radicals. It is also promoted by operating at temperatures over 55 °C with a characteristic release of oxygen bubbles when a solution containing this compound is heated according to Eq. (5).

$$H_2SO_5 + H_2O \rightarrow H_2SO_4 + O_2 + 2H^+ + 2e^- \quad (5)$$

So, for an efficient production is required to skip out the heating of the electrolyte and, as for many other oxidants produced electrochemically, it is also required to prevent the concurrent production of scavengers in the electrolyte, among which ozone and hydrogen peroxide stand out. These oxidants interact with the peroxocompounds producing radicals that end up in the unproductive formation of oxygen.

Structure of the diamond coating affects significantly to the efficiency in the production of oxidants. Inputs such as the sp^3/sp^2 ratio, morphological structure of the diamond surface and doping level can raise or decrease the efficiency of the overall process. Regarding the morphology and the BDD film grain size, chemical vapor deposition (CVD) operational conditions are determinants for the obtention of micro (MD), nano (ND), or ultrananocrystalline (UND) morphology [7–10]. While MD films present grain sizes larger than 1 μM and high roughness, ND and UND present a smoother morphology due to the smaller grain sizes between 10 nm and 1 μM for the first case and lower than 10 nm for the second [9,10]. Besides, the sp^2-bonded carbon amount is higher in films with smaller grains because it is trapped in the grain boundaries or structural defects, which may also affect the material electrochemical performance [11].

Considering that, in this work the performance of two novel diamond coatings nanocrystalline diamond (ND) and ultrananocrystalline diamond (UND) is going to be compared to that of a well-known commercial standard that shows outstanding performance. The oxidant production will be tested at two different current densities and a very exhaustive chemical and electrochemical characterization will be made, in order to understand the impact of the changes introduced in the new coatings on the production of the Caro's acid.

2. Materials & methods

2.1. Diamond coatings

The commercial microcrystalline boron-doped diamond electrode was purchased from Adamant (Switzerland). Boron-doped nanodiamond (ND) and Boron-doped ultra-nanodiamond (UND) were deposited by hot-filament chemical vapor deposition technique (HF-CVD) using a gas of 200 sccm with a mixture of CH_4, and H_2 and B_2O_3 dissolved in methanol as boron source with B/C ratio of 30,000 ppm. The ratio of the gas mixture followed the previous publications of our research group for ND [12] and UND, including the Ar dilution [13,14]. The pressure and temperature were maintained at 650 °C and 30 Torr during the 7 h of growth. In the specific case of ND, the commercial titanium sheet (25 × 25 × 1.5 mm) used as substrate was pretreated before the growth with diamond powder following the methodology described by Oishi et al [15]. On the other hand, the substrate used as a + s for the UND growth was the TiO_2 nanotubes acting not only as a mold above the Ti sheet (25 × 25 × 1.5 mm) (providing a higher electroactive surface) but eliminate the need for pre-treatment, as used in conventional diamond samples [13,14].

2.2. Physical characterization

The quality of the electrodes and their features were evaluated by Raman spectroscopy using a 514 nm laser and bands of interest were fitted using Lorentzian curves according to [12]. In addition, the electrodes were evaluated by SEM to guarantee a film without cracks or delamination (not shown).

2.3. Electrochemical characterization

Electrochemical surface area of the electrodes was estimated by means of cyclic voltammetry in a redox pair presence (ferrocyanide/ferricyanide 1 mM) by the application of a fitted linear equation obtained to anodic peak current plot versus the square rote of scan rate at the Randles-Sevcik equation according to Mei et al. [16]. Furthermore, polarization curves were recorded in 1.0 M H_2SO_4 for the electrodes, and Tafel analysis were conducted.

2.4. Caro's acid production

The peroxymonosulphuric production with the three studied electrodes was evaluated using a 3D-printed electrochemical cell, where the diamond films with a geometrical area of 3.0 cm^2 were set as the anode and steel as the cathode. Both sides were separated by a spacer and the flow inside the electrochemical cell was maintained upwards to promote the interaction of the electrode total area with the BDD surface. The temperature was also controlled at 25 °C, the flux was kept at 50 L h^{-1} and the total volume used was 0.35 L of 1.0 M H_2SO_4. Two current densities were applied: 25 and 300 mA cm^{-2} and the Caro's acid produced was measured by iodometric titration. Additionally, the experimental results were fitted using a proposed phenomenological model. Tests with the same conditions applied for Caro's acid generation were performed with 0.1 g/L of salicylic acid to quantify the hydroxyl generation produced by the different electrodes, following the methodology reported in literature [17]. By this method, the degradation pathway promoted by the anode is the key to the quantification and provides information about the kinetic of the oxidant production.

3. Results and discussion

3.1. Physical and electrochemical characterization

According to literature [18–22], the reactions occurring at the surface of BDD anodes can be influenced by features related to the material

synthesis, particularly graphitic type carbon (sp^2) content, grain size and disorder degree of coating which is also expect to direct affect electrochemical properties such as electrochemical active surface area and oxygen evolution reaction overpotential. These differences can affect the amount of hydroxyl radicals generated and that can help to clarify the behavior of diamond coatings anodes during the application for oxidants electrosynthesis.

Firstly, Raman measurements were carried out with the aim of attest to the quality of diamond films as well as to evaluate the differences in diamond films composition. Fig. 2a. shows that Raman spectra obtained for the studied electrodes are rather different. As can be seen, the characteristic diamond signature, attributed to carbon sp^3 bond at 1,333 cm^{-1} [9] is evident for commercial and ND anode, while for UND this diamond signal is completely hidden by the D band [23,24]. Moreover, for the commercial anode, the sp^3 peak presents Fano asymmetry (a common feature for doped microcrystalline diamonds) [25], however for the ND electrode, only a small signal is presented due to the interference caused by the D band. The D-band can be related to sp^2-bonded carbon atoms in aromatic rings and is also present in the commercial coating [9]. Regarding the G band, which is also a sp^2 signature attributed to vibrations in chain or ring configuration, it appears in different intensities according to the electrode: UND > ND > commercial. Additional signals attributed to the vibration of C—H and C═C stretching vibration modes in *trans*-polyacetylene (TPA) can be also visualized in the Raman spectra of electrodes [26–28].

Once ratio of non-diamond to diamond carbon (i.e. sp^3/sp^2 ratio) cannot be calculated for all electrodes, since sp^3 band is not present significantly for UND anode compared to sp^2 presence and due to the high degree of amorphization, other strategies were used to better understand the diamond features [29]: i) the ratio between the peak D intensity and peak G intensity (ID/IG) that can be helpful to analyze the film disorder related to the impurity presence in diamond films and, ii) the peak G position that allows the analysis of graphitic agglomerates in grain boundaries (Fig. 1c).

As expected, in Fig. 2b it is clear to note that the ID/IG ratio tends to increase with the decrease in the grain size, which indicates higher disorder for ND and UND coatings as compared to commercial one. This result agrees with other studies from literature that reports that the disorder of the diamond coating increases with decrease in the grain size [30,31]. Further, although the commercial electrode has a microcrystalline feature very clearly, as pointed out by the sp^3 diamond band, and lower disorder if compared with the other films, the small D peak and the presence of a G band indicates that the film presents graphitic content in the grain boundaries. The upshifting of the G band position, perceived to the commercial film (1,556 cm^{-1}) from the UND (1,587 cm^{-1}), reveals an increase in the number of aromatic rings and the size of the sp^2-bonded carbon located at grain boundaries.

Furthermore, taking into account previous studies [13,32] the two performed analyses can also provide information about the conductivity of the material: the increase of ID/IG and the upshift of the G band for films with sp^2 contend, may reflect the increase of the material conductivity. Besides the higher conductivity, the presence of sp^2 in diamond films can provide different features like more active sites on the surface, that can affect the electrode performance in different electrochemical applications. In addition, some studies in the literature suggests that electrodes with higher sp^2 content can be more effective in persulfate production [33].

The electrochemical behavior of diamond coatings was initially evaluated by CV measurements in redox couple $[Fe(CN)_6]^{4+/3+}$ at a potential scan rate of 50 mV s^{-1} (Fig. 3). During this measurement, the redox couple is used as a marker to evaluate the electrode behavior, in both cathodic and anodic potential regions, by the electron transfer reaction that occurs at the active sites on BDD's surface [34]. As result, typical well-defined redox peaks can be visualized for the three electrodes and similar values around 1.3 for Ipa/Ipc ratio (the ratio between anodic and cathodic peaks), indicates a quasi-reversible system. In addition, the UND and ND electrode presented smaller separation between the anodic and cathodic peaks (also known as ΔEp) in comparison to commercial one, which means that fabricated coatings present faster electron transfer kinetics.

Then, to further explore the electro transfer process for all electrodes, CVs were recorded at several scan rates ranging from 5 to 500 mV s^{-1} and, by the linear relationship between square root of the scan rate and the anodic current intensity. From these results it is possible to verify that: i) the process is diffusion-controlled, and ii) the UND electrode followed by the ND presents higher slope, reflecting in the better electron transfer for these electrodes.

In addition, using the fitted slope and applying this value to the

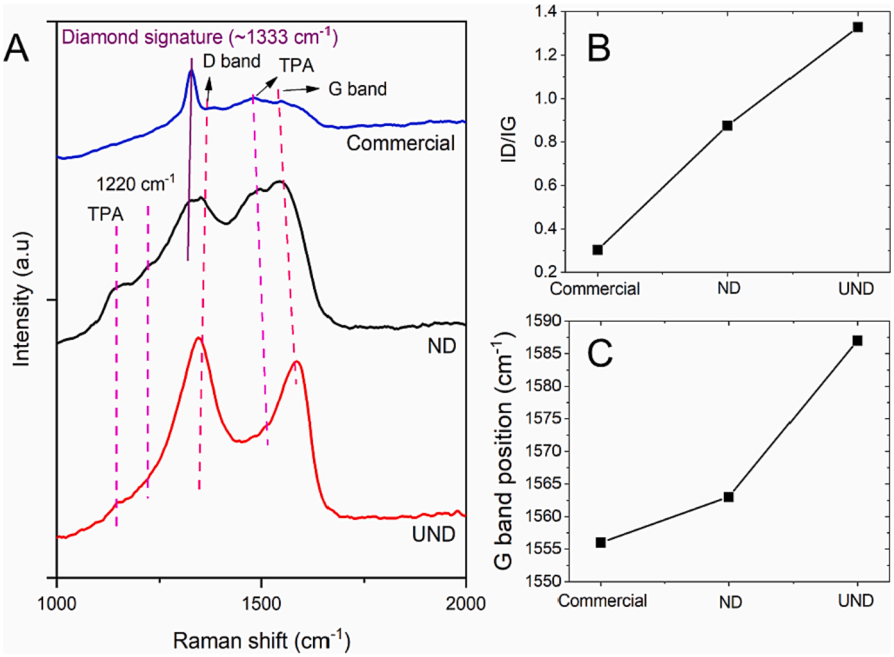

Fig. 2. A) Raman spectra, B) ID/IG and C) G band position for commercial, ND and UND electrodes.

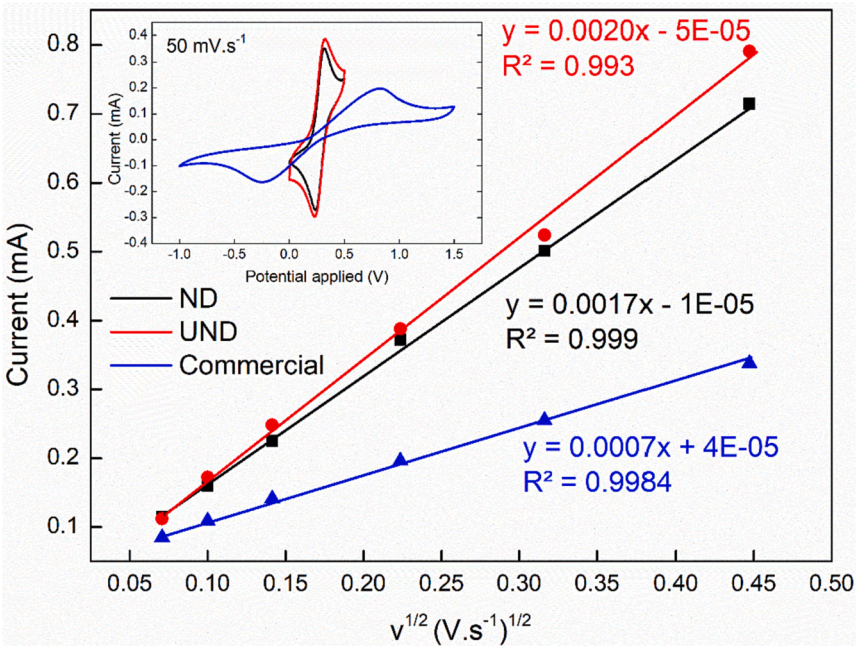

Fig. 3. (A) Square root of the scan rate and the current intensity for the studied electrodes and the different CV shapes obtained for the electrodes (inset).

Randles-Sevcik equation [16], an important feature that is electrochemical area can be obtained. As can be seen higher electrochemical area values were obtained for UND (2.9 cm^2) and ND (1.69 cm^2) compared to the commercial electrode (1.1 cm^2; this result indicates the presence of more active sites for the reactions occurring at the UND and ND surface and is a result expected from porous electrodes [16,35].

3.2. Caro's acid production

Fig. 4 shows the results obtained for Caro's acid production at two different current densities (25 and 300 mA cm^{-2}) using the three different electrodes at the two current applied. In both cases, the charge applied per volume of electrolyzed solution was the same. In the operation at soft conditions, that is low current density (25 mA cm^{-2}), it is interestingly to note that manufactured UND and ND electrodes were more efficient for Caro's acid production than commercial electrode following this order: UND > ND > Commercial. On the other hand, when current is increased to 300 mA cm^{-2}, the production of Caro's acid for commercial electrode within hasher conditions is improved and tend to increase with time, while for ND electrode the production of oxidant is drastically reduced and for UND is slightly lower than results obtained at lower current density.

It is worth to comment that at the beginning of the reaction, when low electric charges are applied, large amounts of species are available for conversion into Caro's acid. However, for longer times (higher applied charges) secondary reactions are responsible for the decomposition of Caro's acid, causing the balance between the degradation and formation rates of the oxidant [36]. This behavior is well documented in the literature and happens because, during electrolysis, not only pure compounds are obtained, but a mixture of oxidants. Under conditions here studied, Caro's acid is the main primary species formed [37], but the occurrence of anodic ozone (Eqs. (6) and (7)), or hydrogen peroxide generated cathodically, cannot be excluded as a secondary species [36,38]. These species can act as scavengers of the primary species (Eqs. (8) and (9)), especially when discontinuous and single-compartment cells are used. It is interesting to point out that these secondary species are difficult to measure, since, as soon as they are formed, they recombine.

$$3H_2O \rightarrow O_3 + 6H^+ + 6e^- \quad (6)$$

$$H_2O + O_2 \rightarrow O_3 + 2H^+ + 2e^- \quad (7)$$

$$O_3 + H_2SO_5 \rightarrow 2O_2 + H_2SO_4 \quad (8)$$

$$O_3 + H_2O_2 \rightarrow 2O_2 + H_2O \quad (9)$$

Then, at the begining of the electrolysis the amount of Caro's acid formed presents similar kinetics, however a steady state value is reached first for commercial electrode while for UND and UNBDD the oxidant achieve a plateau at higher electrolysis time, which is expected since more active sites are available at the surface of these electrode. Same can be observed at 300 mA cm^{-2}, where differenciation is clearly noted after 1.3 Ah L^{-1}.

Knowing that feasibility of a persulfate electrogeneration system will depends on the energy requirements, two important parameters can be determined from the data in Fig. 4, which are the faradaic current efficiency and energy consumption per mM of Caro's acid generated. Fig. 5a. shows the current efficiency obtained by the fitting of experimental data to a single phenomenological model that considers formation and degradation of the sulphate species at the different conditions. The Petersen matrix of this model is shown in Table 1. This model considers two processes occurring at the anode surface: 1) the formation of Caro's acid and 2) the oxygen evolution reaction. In these processes η represent de current efficiency (i.e the percentage of current used in each process and sum of both must be equal to 1). Regarding processes occurring at the bulk, the model considers the Caro's acid decomposition generating oxygen and sulfuric acid following a first order kinetics (with K as kinetic constant). Table 2 shows the parameters obtained after fitting experimental results and the good reproducibility of the proposed model fitted (r^2 ranging from 0.93 to 0.99).

As can be seen in Fig. 5a best current efficiencies are obtained at 25 mA cm^{-2}, which indicates that increasing the current density favors the O_2 side reaction and scanvenger reactions for all anodes. By comparing the efficiency of each anode, it is clear to note the outstanding results achieved by UND coating, which current efficiency values approaching 1 with null waste of current in secondary reactions.

As expected for electrochemical processes, the three electrodes showed an increase in energy consumption with the rise of the charge in the process, regardless of the current applied (Fig. 5b-c). Besides, it is

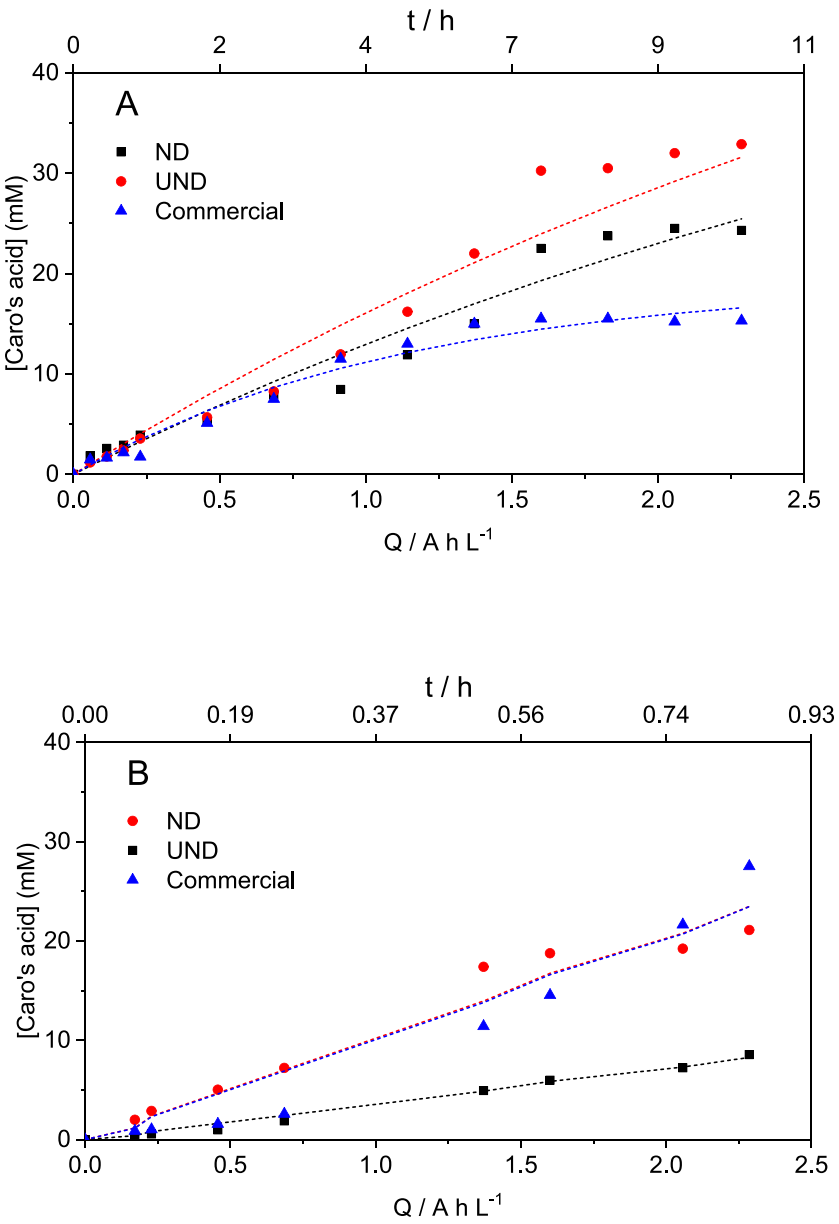

Fig. 4. Caro's acid generation using the three diamond electrodes at A) 25 mA cm^{-2} and B) 300 mA cm^{-2}. Dashed lines are for modelling data.

clear that the ND and UND electrodes have lower consumption compared to commercial electrode in both current densities. When the consumption per oxidant produced is analyzed, it is confirmed that the commercial electrode is the one that needs the highest charge for greater production of Caro's acid. In addition, the UND, in addition to generating more oxidants, also allows this generation at lower consumption.

To understand the mechanisms involved on the Caro's acid production, the electrochemical behavior of 1.0 M H_2SO_4 at surface of the different BDD anodes was investigated by means of polarization curves (Fig. 6a). The oxygen evolution potential (OEP) for the UND electrode was around 1.9 V *vs.* Ag/AgCl) which is much lower as compared to ND (2.1 V *vs.* Ag/AgCl) and commercial diamond coating (2.2 V *vs.* Ag/AgCl)). The obtention of Tafel slopes (inset Fig. 6b) from these curves provides valuable information related to individual processes occurring at the anode's surface during the oxidation of sulfuric acid to Caro's acid. Interestingly, Tafel plots shows that two processes are happening for UND anode: the first corresponding to oxidation of sulfuric acid to peroxymonosulphuric acid and the second correspond to oxygen evolution reaction. On the contrary, for ND and commercial anode just one slope can be visualized and is not possible to discern two processes, which indicates that formation of hydroxyl radicals [22,39] is favored at these anodes and occurs concomitantly with Caro's acid formation.

This difference is accordance with the results from bulk electrolysis, where UND electrode outperformed ND and commercial anode at 25 mA cm^{-2} since at this condition the direct oxidation of sulfuric acid to Caro's acid is promoted, which is also explained by the high surface area of this anode providing more active sites for this reaction to occur in a direct way. In addition, it is important to highlight that the generation of H_2SO_5 production under the best conditions follows the trend of sp^2 content shown by Raman, that is, electrode with high sp^2 content favor direct oxidation of sulfuric acid while higher sp^3 in the electrodes content favor indirect oxidation by the higher amount of $^{\bullet}OH$ radicals generated [9]. To confirm this hypothesis, the production of $^{\bullet}OH$ was evaluated for each diamond coating and the results are presented in Fig. 7.

The quantification of $^{\bullet}OH$ (Fig. 7) was performed in perchloric acid (1 M) due to the incompatibility of the technique when using 1 M H_2SO_4, since previous analyses suggested that the high acid concentration and

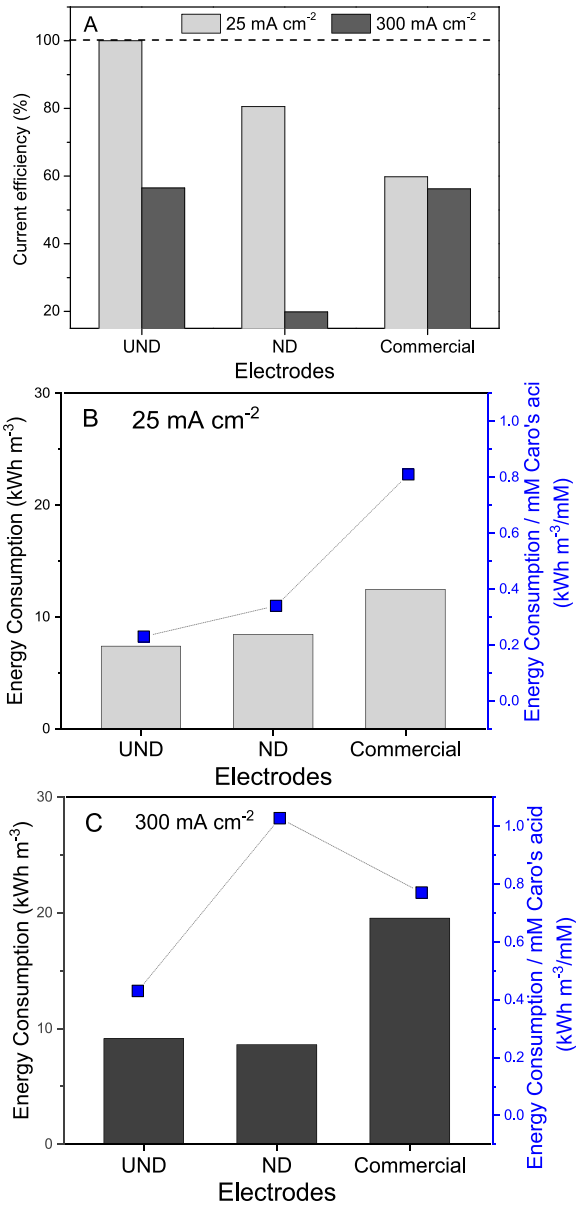

Fig. 5. A) Current efficiency (%) and B) overall energy consumption and energy consumption per mM of Caro's acid at 25 mA cm^{-2} and C) 300 mA cm^{-2} for the three diamond electrodes.

Table 1
Petersen matrix for the production of Caro's acid.

Process/species	S1	S2	S3	Kinetics
Caro's acid production	−1	+1		$I/n_1F{\cdot}\eta$
Water oxidation			+1	$I/n_2F{\cdot}(1\text{-}\eta)$
Caro's acid decomposition		−1	+1	$K[S_2]$

Abbreviations: Specie 1(S1): sulphuric acid; Specie 2 (S2): peroxymonosulphuric acid; Specie 3 (S3): oxygen.

affinity of the electrodes for H_2SO_5 production led to a preferential scavenger reaction of $^{\bullet}OH$ produced to form H_2SO_5, then the salicylic acid is attacked by this oxidant instead of by the $^{\bullet}OH$ as expected. Also, it is possible to observe that, unexpectedly, the ND electrodes produce a greater amount of $^{\bullet}OH$ at lower current density compared to both UND and commercial anode. Conversely, at higher current density, the commercial electrode outperforms the production of $^{\bullet}OH$ radicals compared to ND coating and UND coating, where the last one present

Table 2
Parameters used in the phenomenological model proposed for Caro's acid production at the surface of different diamond coatings.

Anode	j (mA cm^{-2})	K	η	r^2
UND	25	9.59E-04	1.0	0.96
ND	25	9.59E-04	0.80	0.96
Commercial	25	9.59E-04	0.60	0.93
UND	300	9.59E-04	0.56	0.98
ND	300	9.59E-04	0.20	0.99
Commercial	300	9.59E-04	0.56	0.96

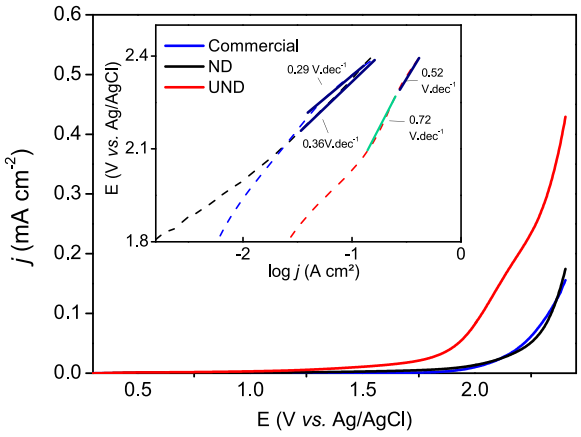

Fig. 6. Polarization curves recorded for the studied electrodes in 1 M H_2SO_4 (inset shows Tafel plots).

almost null production of $^{\bullet}OH$ radical. These results point out that the production of H_2SO_5 at surface of ND and commercial coating are mainly mediated by the $^{\bullet}OH$ generated and follows the trend: the higher hydroxyl production the higher is the amount of H_2SO_5 accumulated with time according to (Eqs. (2)–(4)). However, a different mechanism is involved in the H_2SO_5 production using the UND electrode, since $^{\bullet}OH$ formation is low at both soft and harsh conditions. This behavior agrees with observed in polarization curves, which indicated a favored direct mechanism for Caro's acid formation at the surface of this anode (Eq. (1)) and Raman spectra (Fig. 1a) which shown a higher amount of sp^2 carbon amongst electrodes studied (D- and G-band related to sp^2 -bonded carbon are much more intense). These results are in agrrement with previous studies that demonstrated that lower amount of sp^3 carbon can also imply on a lower amount of $^{\bullet}OH$ since BDDs with higher diamond/graphite (sp^3/sp^2) carbon ratios showed better outcomes in terms of target pollutant degradation than those with higher amount of sp^2 carbon [40,41]. Aslo, despite the direct mechanism is involved in the H_2SO_5 production using the UND electrode the higher electrochemical surface area of this anode due to the its high porosity also contributes to the better outcomes in terms of the Caro's acid formation achieved by using this anode.

Finally, it is interesting to note that the results depicted in Fig. 7 agrees with Tafel analysis: higher Tafel slope indicates that production of $^{\bullet}OH$ is unfavored at the surface of UND electrode as compared to ND and commercial coatings. Based on the results obtained in this study, the potentiality of the application of the UND electrode in the electrochemical generation of the oxidant H_2SO_5 is evident. In addition, it is interesting to highlight that the Caro's acid production generation in the best condition follows the sp^2 contend trend showed by Raman, in accordance with the previous literature report.

4. Conclusions

From this work, the following conclusions can be drawn:

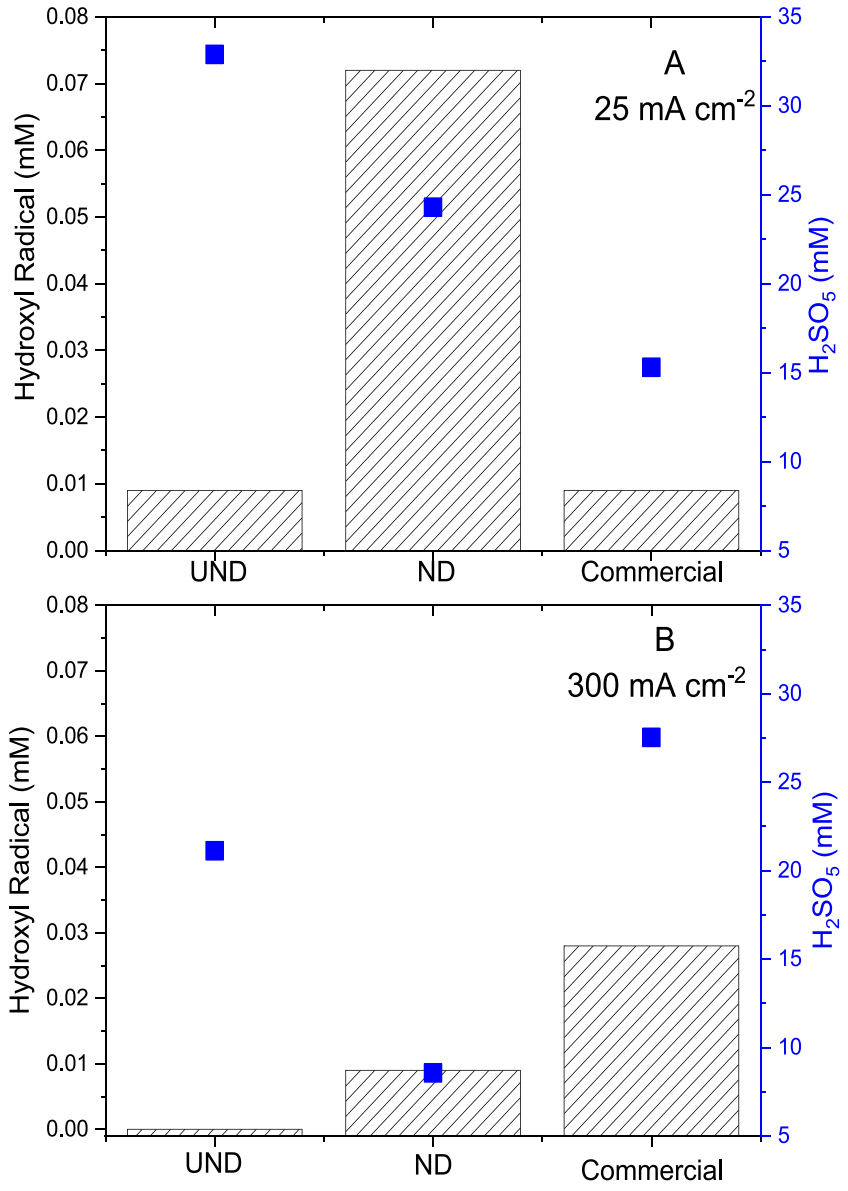

Fig. 7. Hydroxyl radical and Caro'acid production for the studied electrodes in current densities 25 and 300 mA cm^{-2}.

- Caro's acid was efficiently produced in a flow reactor equipped with three different diamond coatings and considerable amounts could be attained at high current efficiencies by operating at low current density (25 mA cm^{-2}), while larger currents led to a decrease in the production of this oxidant because of the promotion of secondary reactions in all cases.
- Among the tested anodes, ultrananocrystalline (UND) electrode were more efficient for Caro's acid production in terms of both current efficiency (approaching 100 % at 25 mA cm^{-2}) and energy consumption (as low as 0.23 kWh m^{-3}/mM Caro's acid). This behavior could be related to the direct oxidation occurring at the surface of this anode as observed by the lower hydroxyl formation among anodes.
- Two factors are also deeply correlated: the high sp^2 content in the UND diamond film (observed by Raman spectra) and its high porosity and electroactive surface area, which in turn provides more active sites for the SO_4 adsorption to form peroxomonosulfuric acid. Tafel slopes corroborates these findings, where more formation of hydroxyl radical is expected at surface of ND and commercial anodes, which presented lower slope valued from Tafel plots.
- Considering the energy consumption and the process efficiency, we can conclude that the UND electrode is more attractive for this application in the studied conditions.

CRediT authorship contribution statement

L.G. Vernasqui: Investigation, Writing – original draft, Methodology, Data curation. **Gessica O.S. Santos:** . **Alberto Rodríguez-Gómez:** Data curation, Methodology, Validation. **Marcos R.V. Lanza:** Formal analysis, Writing – review & editing. **N.G. Ferreira:** Conceptualization, Funding acquisition, Supervision, Writing – review & editing. **M.A. Rodrigo:** Conceptualization, Funding acquisition, Supervision, Writing – review & editing.

Declaration of competing interest

The authors declare that they have no known competing financial interests or personal relationships that could have appeared to influence the work reported in this paper.

Acknowledgements

This work comprises the research project PID2022-138401OB-I00 granted by MCIN/AEI/10.13039/501100011033/ and "Unión Europea Next GenerationEU/PRTR". The authors also acknowledge the financial support provided by Brazilian funding agencies including the Brazilian National for Scientific and Technological Development (CNPq - grant #303943/2021-1) and São Paulo Research Foundation (FAPESP - grants #2021/07615-7, #2019/00592-1, #2017/10118-0, #2020/02743-4 and #2022/03386-6).

References

[1] E. Lacasa, S. Cotillas, C. Saez, J. Lobato, P. Cañizares, M. Rodrigo, Environmental applications of electrochemical technology. What is needed to enable full-scale applications? Curr. Opin. Electrochem. 16 (2019) 149–156.
[2] K.G. Serrano, A critical review on the electrochemical production and use of peroxo-compounds, Curr. Opin. Electrochem. 27 (2021) 100679.
[3] M.P. Castro, M.A. Montiel, I.F. Mena, J. Gäbler, H. King, C. Sáez, M.A. Rodrigo, Outstanding productions of peroxymonosulfuric acid combining tailored electrode coating and 3D printing, J. Water Process Eng. 53 (2023) 103902.
[4] D.L. Ball, J.O. Edwards, The kinetics and mechanism of the decomposition of Caro's acid. I, J. Am. Chem. Soc. 78 (1956) 1125–1129.
[5] K. Serrano, P.A. Michaud, C. Comninellis, A. Savall, Electrochemical preparation of peroxodisulfuric acid using boron doped diamond thin film electrodes, Electrochim. Acta 48 (2002) 431–436.
[6] K. Groenen-Serrano, A critical review on the electrochemical production and use of peroxo-compounds, Curr. Opin. Electrochem. (2020).
[7] P. May, J.N. Harvey, J. Smith, Y.A. Mankelevich, Reevaluation of the mechanism for ultrananocrystalline diamond deposition from Ar/ CH4/ H2 gas mixtures, J. Appl. Phys. 99 (2006).
[8] P.W. May, Y.A. Mankelevich, From ultrananocrystalline diamond to single crystal diamond growth in hot filament and microwave plasma-enhanced CVD reactors: a unified model for growth rates and grain sizes, J. Phys. Chem. C 112 (2008) 12432–12441.
[9] B. Gomez-Ruiz, N. Diban, A. Urtiaga, Comparison of microcrystalline and ultrananocrystalline boron doped diamond anodes: Influence on perfluorooctanoic acid electrolysis, Sep. Purif. Technol. 208 (2019) 169–177.
[10] A.J. Dos Santos, G.V. Fortunato, M.S. Kronka, L.G. Vernasqui, N.G. Ferreira, M. R. Lanza, Electrochemical oxidation of ciprofloxacin in different aqueous matrices using synthesized boron-doped micro and nano-diamond anodes, Environ. Res. 204 (2022) 112027.
[11] F. Souza, C. Saéz, M.R.D.V. Lanza, P. Cañizares, M. Rodrigo, The effect of the sp3/ sp2 carbon ratio on the electrochemical oxidation of 2, 4-D with p-Si BDD anodes, Electrochim. Acta 187 (2016) 119–124.
[12] J.W. Ager III, D.K. Veirs, G.M. Rosenblatt, Spatially resolved Raman studies of diamond films grown by chemical vapor deposition, Phys. Rev. B 43 (1991) 6491.
[13] L. Vernasqui, A. Sardinha, S. Oishi, N. Ferreira, Nanoscale control of high-quality boron-doped ultrananodiamond on dioxide titanium nanotubes as a porous composite, J. Mater. Res. Technol. 12 (2021) 597–612.
[14] L.G. Vernasqui, B.A. Kawata, A. Sardinha, M.A. Rodrigo, N.G. Ferreira, Achievement and electrochemical responsiveness of advanced boron-doped ultrananocrystalline diamond on highly ordered titanium dioxide nanotubes, Diam. Relat. Mater. 121 (2022) 108793.
[15] S.S. Oishi, L.M. Silva, E.C. Botelho, M.C. Rezende, C.A.A. Cairo, N.G. Ferreira, Influence of modified carbon substrate on boron doped ultrananocrystalline diamond deposition, Mater. Res. Express 5 (2018) 026405.
[16] R. Mei, Q. Wei, C. Zhu, W. Ye, B. Zhou, L. Ma, Z. Yu, K. Zhou, 3D macroporous boron-doped diamond electrode with interconnected liquid flow channels: a high-efficiency electrochemical degradation of RB-19 dye wastewater under low current, Appl Catal B 245 (2019) 420–427.
[17] J.-F. Jen, M.-F. Leu, T.C. Yang, Determination of hydroxyl radicals in an advanced oxidation process with salicylic acid trapping and liquid chromatography, J. Chromatogr. A 796 (1998) 283–288.
[18] P. Cañizares, C. Sáez, A. Sánchez-Carretero, M. Rodrigo, Influence of the characteristics of p-Si BDD anodes on the efficiency of peroxodiphosphate electrosynthesis process, Electrochem. Commun. 10 (2008) 602–606.
[19] Y. Einaga, J.S. Foord, G.M. Swain, Diamond electrodes: diversity and maturity, MRS Bull. 39 (2014) 525–532.
[20] C. do Nascimento Brito, D.M. de Araujo, C.A. Martinez-Huitle, M.A. Rodrigo, Understanding active chlorine species production using boron doped diamond films with lower and higher sp3/sp2 ratio, Electrochem. Commun. 55 (2015) 34–38.
[21] S. Garcia-Segura, E.V. Dos Santos, C.A. Martínez-Huitle, Role of sp3/sp2 ratio on the electrocatalytic properties of boron-doped diamond electrodes: a mini review, Electrochem. Commun. 59 (2015) 52–55.
[22] G.O. Santos, K.I. Eguiluz, G.R. Salazar-Banda, C. Saez, M.A. Rodrigo, Understanding the electrolytic generation of sulfate and chlorine oxidative species with different boron-doped diamond anodes, J. Electroanal. Chem. 857 (2020) 113756.
[23] H. Kuzmany, R. Pfeiffer, N. Salk, B. Günther, The mystery of the 1140 cm− 1 Raman line in nanocrystalline diamond films, Carbon 42 (2004) 911–917.
[24] H. Zeng, A.R. Konicek, N. Moldovan, F. Mangolini, T. Jacobs, I. Wylie, P. U. Arumugam, S. Siddiqui, R.W. Carpick, J.A. Carlisle, Boron-doped ultrananocrystalline diamond synthesized with an H-rich/Ar-lean gas system, Carbon 84 (2015) 103–117.
[25] R. Locher, J. Wagner, F. Fuchs, M. Maier, P. Gonon, P. Koidl, Optical and electrical characterization of boron-doped diamond films, Diam. Relat. Mater. 4 (1995) 678–683.
[26] A.C. Ferrari, J. Robertson, Raman spectroscopy of amorphous, nanostructured, diamond–like carbon, and nanodiamond, Philos. Trans. R. Soc. London Series A: Math. Phys. Eng. Sci. 362 (2004) 2477–2512.
[27] P.K. Chu, L. Li, Characterization of amorphous and nanocrystalline carbon films, Mater. Chem. Phys. 96 (2006) 253–277.
[28] V. Mortet, A. Taylor, Z.V. Živcová, D. Machon, O. Frank, P. Hubík, D. Trémouilles, L. Kavan, Analysis of heavily boron-doped diamond Raman spectrum, Diam. Relat. Mater. 88 (2018) 163–166.
[29] A.C. Ferrari, J. Robertson, Resonant Raman spectroscopy of disordered, amorphous, and diamondlike carbon, Phys. Rev. B 64 (2001) 075414.
[30] I. Nasieka, V. Strelchuk, Y. Stubrov, M. Boyko, S. Dudnik, K. Koshevoy, Strel'nitskij, V.,, Comprehensive evaluation of the properties of nanocrystalline diamond coatings grown using CVD with E/H field glow discharge stabilization, J. Nanomater. 16 (2015) 286.
[31] P. Ajikumar, K. Ganesan, N. Kumar, T. Ravindran, S. Kalavathi, M. Kamruddin, Role of microstructure and structural disorder on tribological properties of polycrystalline diamond films, Appl. Surf. Sci. 469 (2019) 10–17.
[32] M. Mertens, I.-N. Lin, D. Manoharan, A. Moeinian, K. Bruehne, H.-J. Fecht, Structural properties of highly conductive ultra-nanocrystalline diamond films grown by hot-filament CVD, Aip Adv. (2017) 7.
[33] J.D.P. Barreto, K. Araujo, D. de Araujo, C. Martinez-Huitle, Effect of sp3/sp2 ratio on boron doped diamond films for producing persulfate, ECS Electrochem. Lett. 4 (2015) (2015) E9–E11.
[34] J.H. Luong, K.B. Male, J.D. Glennon, Boron-doped diamond electrode: synthesis, characterization, functionalization and analytical applications, Analyst 134 (2009) 1965–1979.
[35] X. Li, H. Li, M. Li, C. Li, D. Sun, Y. Lei, B. Yang, Preparation of a porous boron-doped diamond/Ta electrode for the electrocatalytic degradation of organic pollutants, Carbon 129 (2018) 543–551.
[36] J. Cai, M. Zhou, Y. Liu, A. Savall, K.G. Serrano, Indirect electrochemical oxidation of 2, 4-dichlorophenoxyacetic acid using electrochemically-generated persulfate, Chemosphere 204 (2018) 163–169.
[37] J. Herrera-Ordonez, The role of sulfate radicals and pH in the decomposition of persulfate in aqueous medium: A step towards prediction, Chem. Eng. J. Adv. 11 (2022) 100331.
[38] P. Cañizares, F. Larrondo, J. Lobato, M. Rodrigo, C. Sáez, Electrochemical synthesis of peroxodiphosphate using boron-doped diamond anodes, J. Electrochem. Soc. 152 (2005) D191.
[39] K.C. de Freitas Araujo, D.R. da Silva, E.V. dos Santos, H. Varela, C.A. Martínez-Huitle, Investigation of persulfate production on BDD anode by understanding the impact of water concentration, J. Electroanal. Chem. 860 (2020) 113927.
[40] E. Guinea, F. Centellas, E. Brillas, P. Cañizares, C. Sáez, M.A. Rodrigo, Electrocatalytic properties of diamond in the oxidation of a persistant pollutant, Appl. Catal. B 89 (2009) 645–650.
[41] D.M. de Araujo, P. Canizares, C.A. Martínez-Huitle, M.A. Rodrigo, Electrochemical conversion/combustion of a model organic pollutant on BDD anode: Role of sp3/ sp2 ratio, Electrochem. Commun. 47 (2014) 37–40.